Available online at www.sciencedirect.com
ScienceDirect
Journal of the European Ceramic Society 30 (2010) 727–736
www.elsevier.com/locate/jeurceramsoc

Microstructure and properties of Co-, Ni-, Zn-, Nb- and W-modified multiferroic $BiFeO_3$ ceramics

Feridoon Azough [a], Robert Freer [a,*], Michael Thrall [a], Robert Cernik [a], Floriana Tuna [b], David Collison [b]

[a] *Materials Science Centre, School of Materials, University of Manchester, Grosvenor Street, Manchester M1 7HS, UK*
[b] *School of Chemistry, University of Manchester, Oxford Road, Manchester M13 9PL, UK*

Received 10 June 2009; received in revised form 9 September 2009; accepted 10 September 2009
Available online 9 October 2009

Abstract

$BiFeO_3$ polycrystalline ceramics were prepared by the mixed oxide route and a chemical route, using additions of Co, ZnO, NiO, Nb_2O_5 and WO_3. The powders were calcined at 700 °C and then pressed and sintered at 800–880 °C for 4 h. High density products up to 96% theoretical were obtained by the use of CoO, ZnO or NiO additions. X-ray diffraction, SEM and TEM confirmed the formation of the primary $BiFeO_3$ and a spinel secondary phase ($CoFe_2O_4$, $ZnFe_2O_4$ or $NiFe_2O_4$ depending on additive). Minor parasitic phases $Bi_2Fe_4O_9$ and $Bi_{25}FeO_{39}$ reduced in the presence of CoO, ZnO or NiO. Additions of Nb_2O_5 and WO_3 did not give rise to any grain boundary phases but dissolved in $BiFeO_3$ lattice. HRTEM revealed the presence of domain structures with stripe configurations having widths of typically 200 nm. In samples prepared with additives the activation energy for conduction was in the range 0.78–0.95 eV compared to 0.72 eV in the undoped specimens. In co-doped specimens (Co/Nb or Co/W) the room temperature relative permittivity was ~110 and the high frequency dielectric loss peaks were suppressed. Undoped ceramics were antiferromagnetic but samples prepared with Co or Ni additions were ferromagnetic; for 1% CoO addition the remanent magnetization (M_R) values were 1.08 and 0.35 emu/g at temperatures of 5 and 300 K, respectively.

Keywords: $BiFeO_3$; Perovskites; Multiferroics

1. Introduction

Multiferroics are materials which exhibit the simultaneous presence of ferromagnetic, ferroelectric and ferroelastic coupled order parameters within a single phase[1,2] (or at least two of these characteristics). The perovskite $BiFeO_3$ is multiferroic, having ferroelectric ordering below the Curie transition temperature $T_c \sim 1103$ K and a G type antiferromagnetic transition at $T_n \sim 643$ K.[3] Extensive neutron and X-ray diffraction studies have shown $BiFeO_3$ to crystallise with a rhombohedral distorted perovskite cell, with space group R3c and unit cell parameters $a = 5.616$ Å and $\alpha = 59.35°$.[4,5]

Attempts to sinter bulk samples have met with limited success with most products containing $Bi_2Fe_4O_9$ and $Bi_{25}FeO_{39}$ secondary phases,[6–8] exhibiting low density multiple valance states of the Fe[9] and high levels of dielectric loss giving poorly saturated ferroelectric hysteresis loops.[3] Strategies to prepare high density, pure single phase $BiFeO_3$ and thus improve the ferroelectric and magnetic properties have included rapid thermal sintering,[3,8] chemical leaching,[10] partial substitution of A-site cation by lanthanide elements[11] and forming solid solution with other type of ABO_3 type perovskites.[12–14] Electrical characteristics of the solid solution samples indicated a slight reduction in the dielectric loss but no significant change in the poorly saturated ferroelectric hysteresis loops.

Recently Jun et al.[15] studied the substitution of Nb for Fe in $BiFeO_3$ and reported a large increase in the electrical resistivity of the polycrystalline ceramics. In addition, Nb-doped $BiFeO_3$ showed very weak remanent polarization and exhibited ferromagnetic-like behaviour. Subsequently Jun and Hong[16] prepared $BiFeO_3$ ceramics co-substituted by niobium and cobalt and reported small structural transitions in the $BiFeO_3$ phase as well as greatly reduced dielectric loss. They found that whilst the

* Corresponding author.
E-mail address: Robert.Freer@manchester.ac.uk (R. Freer).

0955-2219/$ – see front matter © 2009 Elsevier Ltd. All rights reserved.
doi:10.1016/j.jeurceramsoc.2009.09.016

undoped ceramic was antiferromagnetic, all the substituted specimens were ferromagnetic. They suggested that doping caused a distortion of the Fe–O octahedra and modification of the antiparallel spin structure.

Hence the occurrence of Bi-rich secondary phases and poor densification hamper the development of high quality $BiFeO_3$ ceramics. It is clear that the secondary phase can be reduced to acceptable levels and densification enhanced by suitable additions. A further obstacle to the characterization of the electrical properties of $BiFeO_3$ ceramics is the high conductivity of the undoped material.

In this study we have investigated the effects of small additions of niobium, cobalt, tungsten, zinc and nickel on the sintering of bulk $BiFeO_3$ samples and the associated microstructure and electrical/magnetic properties. In order to avoid disturbing the delicate balance between Bi and Fe, which affects secondary phase formation during sintering[1] we did not use direct substitutions for Fe but explored the effect of the addition to the stoichiometric $BiFeO_3$ powder. Our additives were CoO, NiO and ZnO used individually, and then in combination with Nb_2O_5 or WO_3. The nominal divalent oxides (Co and Ni) will yield higher valence species during the sintering process and this is important for the final products.

Recognising the potential importance of domain structures in multiferroic materials we have undertaken TEM studies of the ceramics. There have been many TEM studies of ferroelectric domain structures in electroceramics with tetragonal structure but comparatively few studies of domain structures in phases with rhombohedral distortions.[17] We have therefore examined by HRTEM the ferroelectric domain configurations in the $BiFeO_3$ ceramics and have analysed the nature of domain walls.

2. Experimental

2.1. Sample preparation

The $BiFeO_3$ specimens were prepared by the mixed oxide route using Bi_2O_3 (≥98%) and Fe_2O_3 (99%). Small additions of CoO (99%), NiO (99%), ZnO(99%), Nb_2O_5 (99%) and WO_3 (99%) were made to yield the following series of samples:

(i) $BiFeO_3$ + 0.4, 0.6, 0.8, 1, and 1.2 wt% excess CoO.
(ii) $BiFeO_3$ + 1 wt% excess NiO.
(iii) $BiFeO_3$ + 1 wt% excess CoO + 0.15, 0.3, 0.4, 0.5 wt% excess Nb_2O_5.
(iv) $BiFeO_3$ + 1 wt% excess CoO + 0.1, 0.2, 0.3 wt% excess WO_3.
(v) $BiFeO_3$ + 1 wt% excess ZnO + 0.3 wt% excess Nb_2O_5.
(vi) $BiFeO_3$ and $BiFeO_3$ + 1 wt% excess CoO prepared by a modified Pechini chemical route.[18]

For the mixed oxide samples the powders were wet milled in propan-2-ol for 16 h, calcined at 700 °C for 4 h and then wet milled again for a further 16 h. Cylindrical samples of 10 mm diameter were pressed at 100 MPa. The pellets were fired at 800–900 °C for 4 h in air, using a heating and cooling rate of 180 °C/h.

For the chemically prepared samples (batch vi) $Fe(NO_3)_3{\cdot}9H_2O$ $Co(NO3)_2{\cdot}5H_2O$ and citric acid were first dissolved in distilled water. The solution was stirred and heated at 70 °C for 3 h to form a sol. Aqueous ammonia was used to adjust the pH to about 1. The required amount of $Bi(NO_3)_3$, to form a ratio of 1:1 of iron and bismuth in the final product, was slowly added to avoid precipitation of $Bi(OH)_3$ in the sol. The sol was dried at 130 °C in an oven to form a gel. The gel was dried in an oven at 200 °C for 24 h then calcined, milled, pressed and fired using the same conditions as for the mixed oxide route.

Product densities were determined from weight and dimension measurements. X-ray diffraction for phase identification employed a Philips X'Pert-MPD in conjunction with Cu Kα radiation. Samples were scanned from 10° to 90° 2θ, in 0.05° steps, using a counting time of 10 s per step. Following identification of the peaks, Rietveld refinement was carried out using the TOPAS[19] refinement programme. The initial atomic coordinates for the $BiFeO_3$ crystal structures were taken from Zhang et al.[9]

For microstructural examination, specimens were ground on 1200 grade SiC and then successively polished on 6, 1 and 0.25 μm diamond paste followed by OPS (colloidal silica suspension) for 5 h. The polished samples were chemically etched using hot, concentrated sulphuric acid. The samples were investigated by scanning electron microscopy using a Philips XL30 FEG SEM.

For the TEM analysis, specimens were first ground on 1200 grade SiC to reduce the thickness to approximately 300 μm. They were ultrasonically cut into 3 mm diameter discs (Model KT150, Kerry Ultrasonic Ltd.) then dimpled (Model D500, VCR Group, San Francisco, USA) to reduce the ceramic disc thickness to 30 μm. Finally the discs were ion beam thinned (using a Gatan precision ion polishing system model 691 (*PIPS*^{TM})) operating at 4–6 kV. TEM analysis was carried out using a Philips CM200 transmission electron microscope (fitted with an EDAX DX4 EDS system) operating at 200 kV and Tecnai G2 FEGTEM operating at 300 kV.

To prepare samples for dielectric measurements, the discs were ground on SiC to reduce the thickness to less than 1 mm and coated with In–Ga, platinum or silver paste. All three coating materials gave similar results. A Hewlett Packard (4192A) Impedance Analyser was used in conjunction with a Carbolite (MTF 9/15/130) tube furnace to determine capacitance, loss tangent and impedance as a function of temperature from room temperature to 500 °C at frequencies of 10 Hz to 10 MHz.

The magnetic properties were determined using a superconducting quantum interferometric device (SQUID), Quantum Design MPMS XL SQUID magnetometer, equipped with a 7 T magnet. Samples were 2.5 mm diameter and 4 mm thick. They were cooled to 0 K under Zero Field Cooled (ZFC) and Field Cooled (FC) conditions. Magnetization measurements were performed between 400 and 0 K.

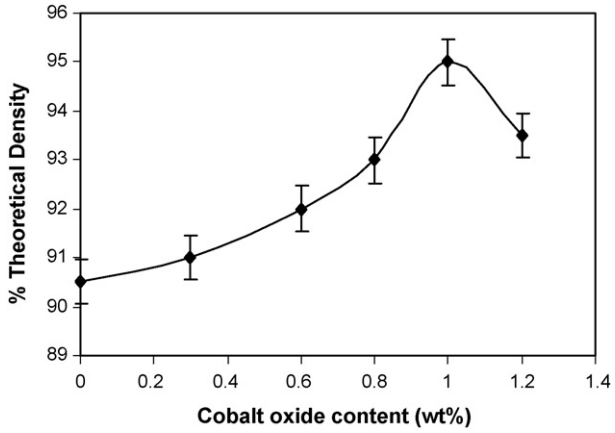

Fig. 1. Densification of $BiFeO_3$ as a function of CoO additions for samples sintered at 800 °C for 4 h.

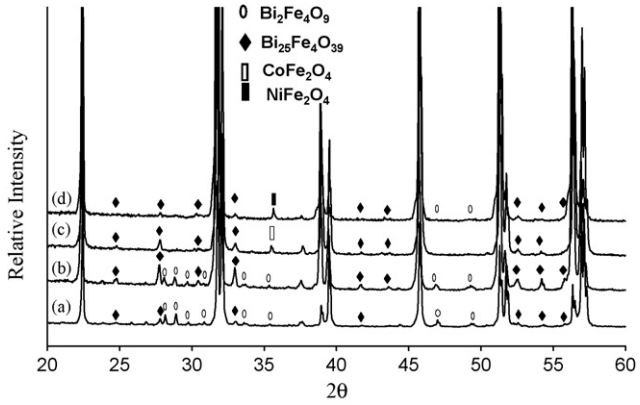

Fig. 2. X-ray diffraction spectra for $BiFeO_3$ specimens: (a) undoped, prepared without calcination, (b) undoped but prepared with calcination step at 700 °C, (c) prepared with calcination step and addition of 1 wt% CoO and (d) prepared with calcination step and addition of 1 wt% NiO.

3. Results and discussion

3.1. Densification

Undoped $BiFeO_3$ is difficult to densify by conventional sintering at 800 °C. Increasing the sintering temperature to 900 °C improved the density to almost 85% theoretical, but the higher volatility of Bi at this temperature moved the samples away from stoichiometry and generated a higher content of $Bi_{25}FeO_{39}$ and $Bi_2Fe_4O_9$ secondary phases. Additions of CoO (0.6–1.0 wt%) to the starting powders enhanced the densification, yielding a maximum density of 95% theoretical, for sintering at 800 °C (Fig. 1). NiO and ZnO additions improved the densification in a similar manner to CoO. It is inferred that the enhancement arose from liquid phase formation, with a composition approaching that of a Bi_2O_3-spinel eutectic, but this could not be confirmed. The addition of Nb_2O_5 or WO_3, up to 0.3 wt%, did not affect the density of Co-doped samples, but higher levels of Nb_2O_5, for example, degraded the products. The focus of the study was therefore samples prepared with single additions of divalent species (Co, Ni, Zn) and co-doping with up to 0.3 wt% higher valance species oxides (Nb or W).

3.2. X-ray diffraction

Fig. 2 shows X-ray diffraction spectra collected for selected $BiFeO_3$ samples. The spectra for the undoped samples (spectra a and b), are very similar, and shows that inclusion of a calcination step (spectrum 2b) enables the maximum sintering temperature to be reduced to 800 °C and leads to greater development of both the $BiFeO_3$ primary phase and the secondary phases: $Bi_{25}FeO_{39}$ and $Bi_2Fe_4O_9$.[20–22] The formation of these secondary phases in $BiFeO_3$ is well documented[6,7,21,22] and has previously proven difficult to eliminate from bulk $BiFeO_3$ samples. Independent studies of bulk $BiFeO_3$ samples prepared by a chemical route (sample series vi) revealed that the levels of secondary phases are significantly less than in typical mixed oxide prepared samples.[6] It has been suggested that minor impurities in the mixed oxide starting powders stabilises the $Bi_{25}FeO_{39}$ phase[7] leading to the formation of $Bi_2Fe_4O_9$ phase to maintain the stoichiometry of $BiFeO_3$.

The spectra for the doped samples in Fig. 2 (spectra c and d) represent $BiFeO_3$ samples which were calcined and sintered with 1 wt% CoO and NiO, respectively. It may be seen that the small additions of cobalt or nickel oxide suppress the formation of $Bi_2Fe_4O_9$. However, lower levels of $Bi_{25}FeO_{39}$ phase were detected in all the doped samples. The use of the divalent additives also gave rise to a minor spinel phase, $CoFe_2O_4$ and $NiFe_2O_4$ in spectra 2c and 2d, respectively. Nevertheless, the content of secondary phases in $BiFeO_3$ prepared with 1 wt% CoO was minimal. This was also the case in samples prepared with 1 wt% CoO (or ZnO), plus Nb_2O_5 or WO_3 (samples series iii, iv and v). The content of secondary phases was much reduced in the doped samples prepared by the chemical route. The X-ray spectra for such samples are not significantly different from those shown in Fig. 2.

The Rietveld refined unit cell parameter (a) and angle (α) for the rhombohedral $BiFeO_3$ structure are shown in Fig. 3 as a function of CoO additions. Two regions can be seen. In region 1, the unit cell parameter (a) decreased with increasing CoO additions, whilst the rhombohedral angle (α) exhibited a small corresponding increase. It is inferred that these changes result from direct substitution of multi-valent Co for the multi-valent Fe within the $BiFeO_3$ structure. As the ionic radius of Co^{3+} (54.5 pm) is smaller than that for Fe^{2+} (61 pm) or Fe^{3+} (55 pm) ions,[22] a small structural contraction can be expected, giving rise to a slight canting of the rhombohedral unit cell. At higher levels of Co additions, above 0.8 wt%, there is minimal change in the lattice parameter (a) and rhombohedral angle (α) (region 2 of Fig. 3), indicating that most of the extra Co is consumed in forming the Co-rich secondary phase, $CoFe_2O_4$. In samples prepared with 1.0 wt% CoO plus either Nb_2O_5 or WO_6 (up to 0.3 wt%) there was a small steady *increase* in lattice parameter as the larger, higher valence ions (W^{6+} = 60 pm, Nb^{5+} = 64 pm) are accommodated in the rhombohedral structure in place of the smaller, predominant iron species, Fe^{3+} (55 pm). In fact the Nb^{5+} and W^{6+} species counteract the shrinkage of the unit cell caused by incorporation of the primary trivalent additive.

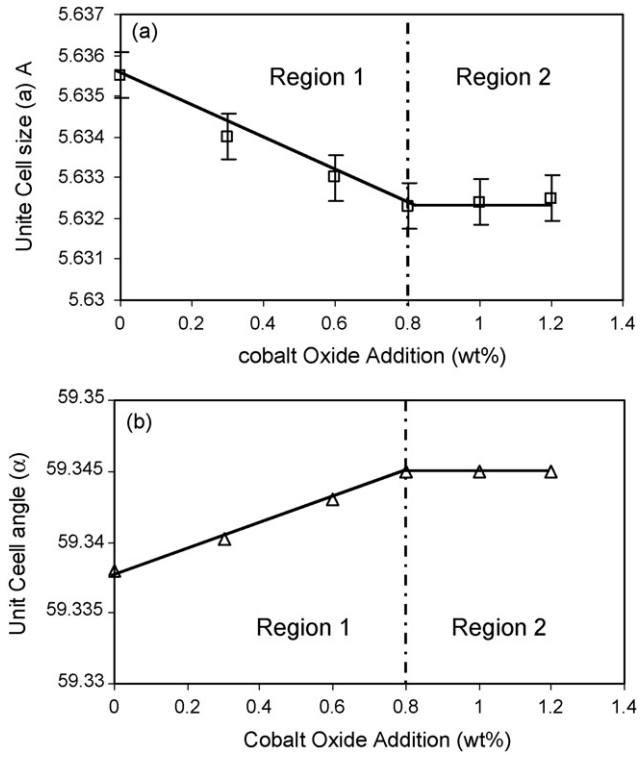

Fig. 3. (a) The rhombohedral lattice parameter and (b) unit cell angle for $BiFeO_3$ as a function of cobalt oxide additions.

3.3. SEM

A typical micrograph for high density $BiFeO_3$ ceramics prepared with 1.0% CoO is presented in Fig. 4a. The average grain size of the matrix is 2–4 μm; this is significantly smaller than in the lower density, undoped samples where grain sizes were 5–10 μm. In addition to the $BiFeO_3$ matrix phase, two secondary phases were identified by X-ray diffraction in Co-added samples, $Bi_{25}FeO_{39}$ and $CoFe_2O_4$. The two latter phases were observed as isolated grains within the $BiFeO_3$ matrix (Fig. 4a). EDS analysis confirmed that the irregularly shaped, dark regions, up to 10 μm in size, were essentially Co–Fe oxides, representing the spinel $CoFe_2O_4$. The lighter coloured, more uniform grains (approximately 2–4 μm in size) were rich in Bi with small amounts of Fe. These grains are probably the $Bi_{25}FeO_{39}$ phase identified by X-ray diffraction. The microstructures of samples prepared with 1.0% NiO or ZnO were very similar to those shown in Fig. 4a, except the larger spinel grains were $NiFe_2O_4$ or $ZnFe_2O_4$ instead of the cobalt analogue. The size of the $CoFe_2O_4$ spinel phase was much smaller and more uniformly distributed in the microstructure of the sample prepared by the chemical route as (Fig. 4b).

When either Nb or W was added with CoO to the $BiFeO_3$ formulation, then there were minor changes to the microstructure (Fig. 4c and d). In addition to the matrix and the large irregular dark spinel grains (mainly $CoFe_2O_4$) there are two Bi-containing minor phases: $Bi_2Fe_4O_9$ and $Bi_{25}FeO_{39}$ (which appear grey in colour). The $Bi_{25}FeO_{39}$ phase is irregular in shape whereas the $Bi_2Fe_4O_9$ phase has faceted boundaries. A higher magnification backscattered electron (BSE) image (Fig. 5) shows the constituent phases in the co-doped $BiFeO_3$ ceramic.

In view of the ambiguity in the interpretation of some of the minor phases, and the identification of a number of interesting microstructural features by SEM, more detailed microstructural investigations were undertaken by TEM.

3.4. Transmission electron microscopy

Thin foil EDS analysis of the matrix confirmed that the ratio of Bi to Fe was very close to one as anticipated for $BiFeO_3$; any

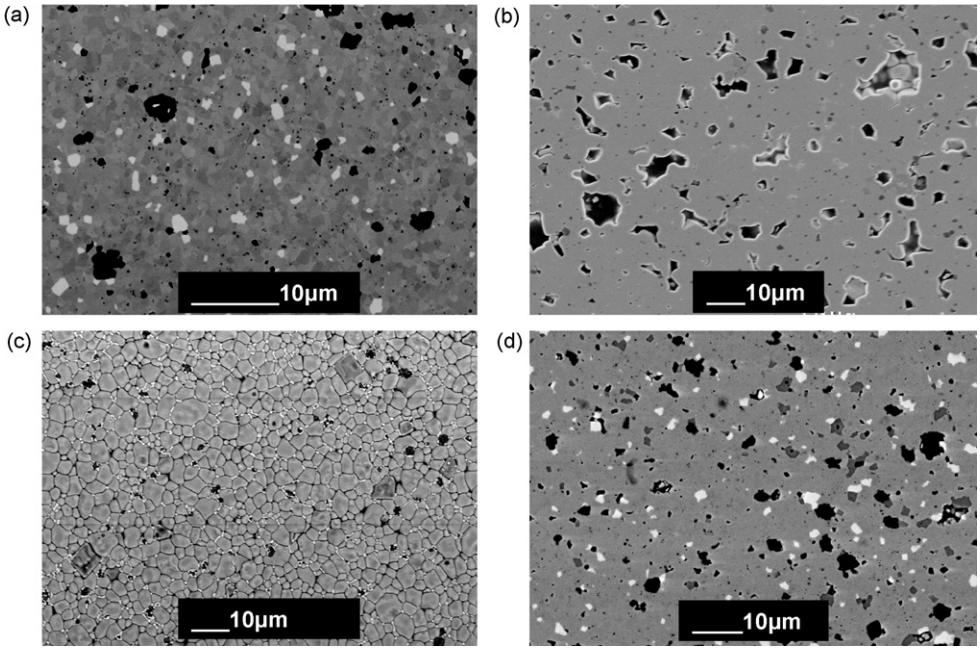

Fig. 4. SEM micrographs for $BiFeO_3$ samples sintered at 800 °C for 4 h: (a) mixed oxide prepared with 1%CoO, (b) chemically prepared with 1%CoO, (c) mixed oxide prepared with 1%CoO + 0.3% Nb_2O_5 and (d) mixed oxide prepared with 1%CoO + 0.2% WO_3.

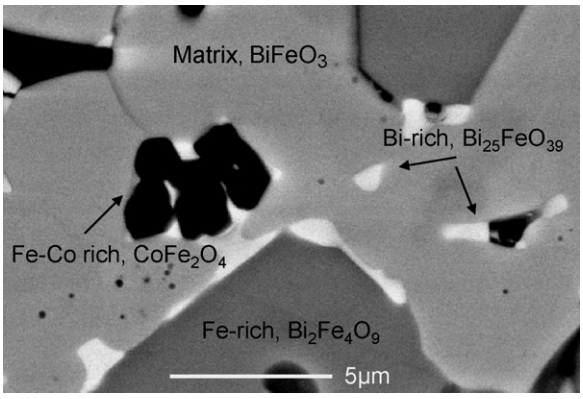

Fig. 5. High magnification backscattered electron image for a sample prepared with 1 wt% CoO and 0.3 Nb_2O_5 showing the constituent phases in the microstructure.

Co in the matrix was below the detection limit of the system (approximately 0.1 wt%).

Fig. 6a is a TEM image of one of the secondary phases. The EDS analysis suggests this is $Bi_{25}Fe_1O_{40}$. There was no evidence of Co in this phase, but a trace of Zr was detected. It is believed that the Zr was an impurity in the starting material (or a containment from the milling process) and acts to stabilise this Bi-rich phase. This clearly suggests that in order to obtain single phase $BiFeO_3$ bulk ceramics the purity should be carefully controlled.

For the secondary phase shown in Fig. 6b only Fe and Co were detected in the EDS spectrum; these were in the ratio 2:1 confirming the presence of the $CoFe_2O_4$ spinel phase. The majority of the Co added to the sample appears to concentrate in the spinel phase. However, the fact that the cell parameters and the magnetic properties (later section) change with Co additions, suggests that some Co does in fact enter the matrix phase.

3.5. Ferroelectric domain structures in $BiFeO_3$

Clear domain structures were identified in the $BiFeO_3$ specimens, for example Fig. 7a. The domain configurations and the nature of domain walls may be analysed on the basis of the predicted twinning planes for the formation of domain walls in the rhombohedral system. The ferroelectric domain walls, which in fact are twining planes, vary with the crystal structure.[17] For a plane (h k l) in the paraelectric phase to become a domain wall in the ferroelectric phase it must have mechanical compatibility to avoid cracking in the rigid body. These are called the *permissible domain walls*. Orientations of the *permissible domain walls* can

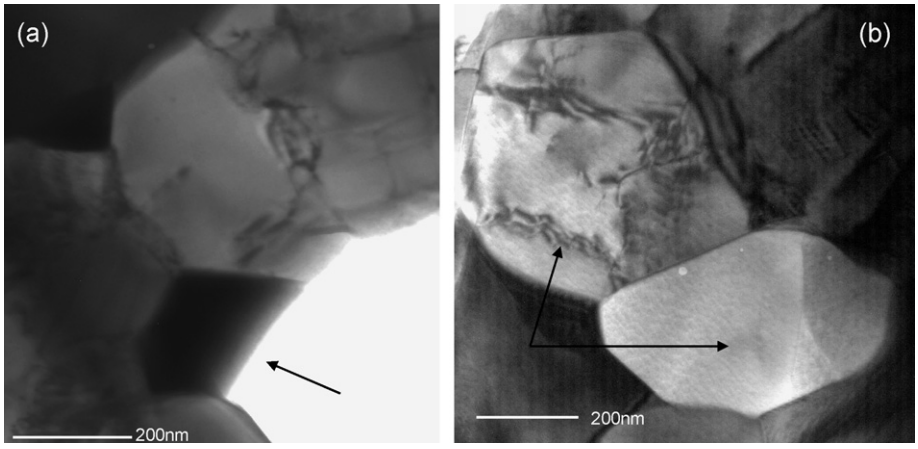

Fig. 6. TEM images of the secondary phases (arrowed) in $BiFeO_3$ prepared with 1 wt% CoO additions: (a) $Bi_{25}FeO_{39}$ and (b) $CoFe_2O_4$.

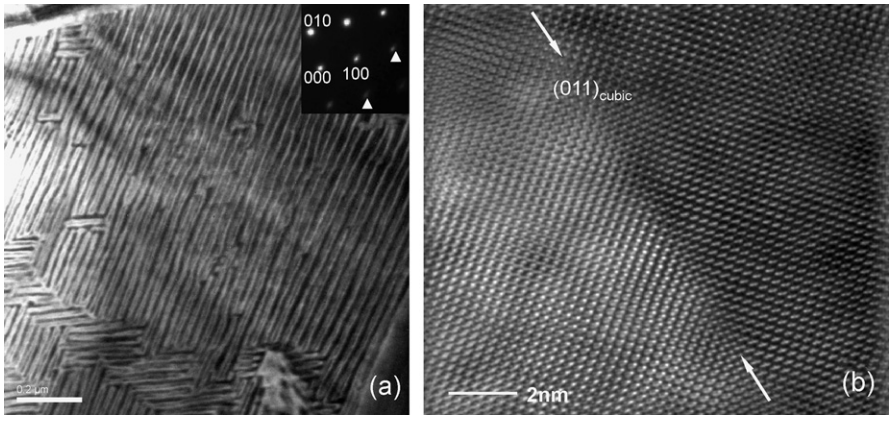

Fig. 7. (a) TEM image of stripe morphology domains in $BiFeO_3$ sample prepared with 1 wt% CoO additions and (b) HRTEM image of domain wall in stripe morphology domains ($BiFeO_3$ prepared with 1 wt% CoO additions).

be predicted for the various pseudo-cubic ferroelectric phases of the perovskite structure.[23]

The polarization vector for the rhombohedral phase lies along <1 1 1>, leading to the formation of eight possible polarization variants. The possible types of domains are 71°, 109° and 180°. These angles are the rotation angles between neighbouring domains. The *permissible domain walls* are therefore {1 1 0} for 109°, {0 0 1} for 71° and any plane parallel to the polarization vector for 180° domains. In a non-perfect crystal, however it can be expected that the actual wall may be slightly misoriented from the predicted planes; the smaller the wall area, the larger is the possible tilt. In a recent study of the $BiFeO_3$–$PbTiO_3$ system, Woodward et al.[24] did not observe ferroelectric domains in the $BiFeO_3$ and suggested the ferrite grains were single domain. However, 71° and 109° types of domains, where the domain boundaries are parallel to (0 0 1) and (1 1 0) planes of the cubic parent phase, have been recently reported for thin film $BiFeO_3$ investigated by HRTEM imaging.[25]

The domain walls observed in the present samples were quite stable under the influence of the electron beam and their size did not vary. Domains with stripe configuration were frequently observed (Fig. 7a). The domain width is typically 200 nm. According to Chen et al.[25] the domain width in $BiFeO_3$ thin films varies from 100 to 350 nm depending on the thickness of the film. The grain in Fig. 7a has been view along the [0 0 1] zone axis and the related electron diffraction pattern is shown as an inset of Fig. 7a. A high resolution transmission electron microscope (HRTEM) image of a stripe domain wall is shown in Fig. 7b. The electron beam is parallel to the [0 0 1] zone axis and the related diffraction pattern is shown in the inset of Fig. 7a; the splitting of the electron diffraction spots perpendicular to the (1 1 0) planes (arrowed) indicates that the domain wall is (1 1 0) type. This can also be seen in the HRTEM image (arrowed in Fig. 7b). Randall and Barber[26] calculated the surface energy of {1 1 0} and {1 0 0} boundaries for the rhombohedral system and found that the energy of {1 0 0} boundaries was three times more than those of {1 1 0} boundaries. In agreement with their prediction, they mainly observed {1 1 0} boundaries for rhombohedral lead zirconium titanate ceramics. We also found {1 1 0} boundaries to be predominant for stripe domains. Chen et al.[25] also reported a higher population of {1 1 0} boundaries in epitaxial (0 0 1) $BiFeO_3$ thin films.

3.6. Electrical and magnetic properties

Fig. 8 shows the electrical conductivity as a function of temperature for $BiFeO_3$ ceramics prepared with and without additives. Following the procedure of Jun and Hong[16] electrical conductivity values were determined from impedance data where the total resistance (grain + grain boundary) was obtained from the intercept of the grain boundary arc with the real axis at the low frequency side of the Cole–Cole plot. With the exception of the conductivity values for undoped samples there was a clear trend of increasing resistance and increasing activation energy as we move from undoped, to a single additive (Co, or Ni or Zn), to double additives (Co plus Nb or W). This behaviour and the activation energy range are broadly consistent with the findings

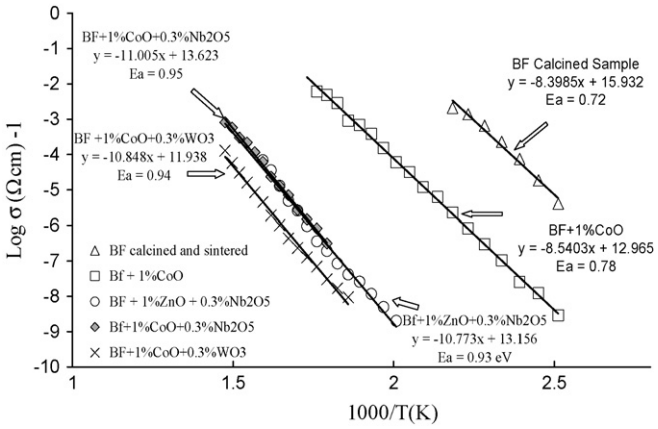

Fig. 8. Temperature dependence of electrical conductivity of $BiFeO_3$ based ceramics: undoped $BiFeO_3$ (△), $BiFeO_3$ + 1% CoO (□), $BiFeO_3$ + 1.0%ZnO + 0.3%Nb_2O_5 (◯), $BiFeO_3$ + 1.0%CoO + 0.3%Nb_2O_5 (♦) and $BiFeO_3$ + 1.0%CoO + 0.3%WO_3 (×).

of Jun and Hong.[16] The use of a combination of additives led to a 25% increase in the activation energy (0.95 eV) compared to the additive-free samples (0.72 eV) and a significant increase in resistivity by almost five orders of magnitude compared to the single doped samples. The minor changes in grain size and second phase content are not sufficient to explain the large changes in resistivity. The incorporation of higher valence state dopants (i.e. W or Nb) in the lattice may be responsible for the increase in resistivity of $BiFeO_3$.

Only in the double additive samples was the resistivity high enough to enable reliable relative permittivity data to be obtained (Fig. 9). The room temperature relative permittivity of ∼110 is comparable with data published for similar samples[16] and the dielectric loss (tan δ) values are less than 1 for temperatures up to 300 °C.

Fig. 10a shows dielectric loss at room temperature as a function of frequency for the undoped and the CoO, ZnO- and NiO-added $BiFeO_3$ samples. Two Debye-like relaxation peaks can be seen in the loss data for all samples. It is inferred that the lower frequency peak is due to interfacial or space charge polarization. The higher frequency relaxation has been attributed to ionic relaxation by Wang et al.;[5] they suggested that the high losses from ionic relaxation are related to the multiple valence

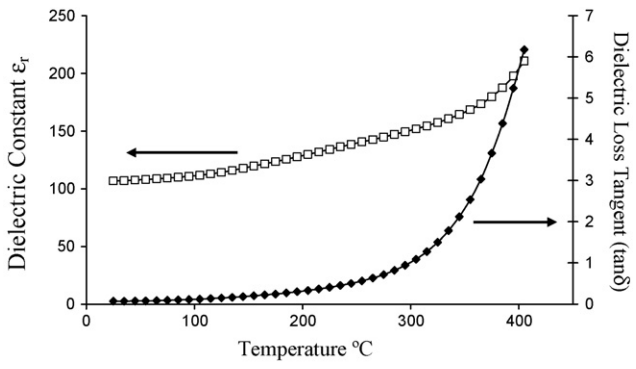

Fig. 9. Dielectric constant and loss tangent (at 100 kHz) as a function of temperature for $BiFeO_3$ prepared with 1%CoO + 0.3%Nb_2O_5.

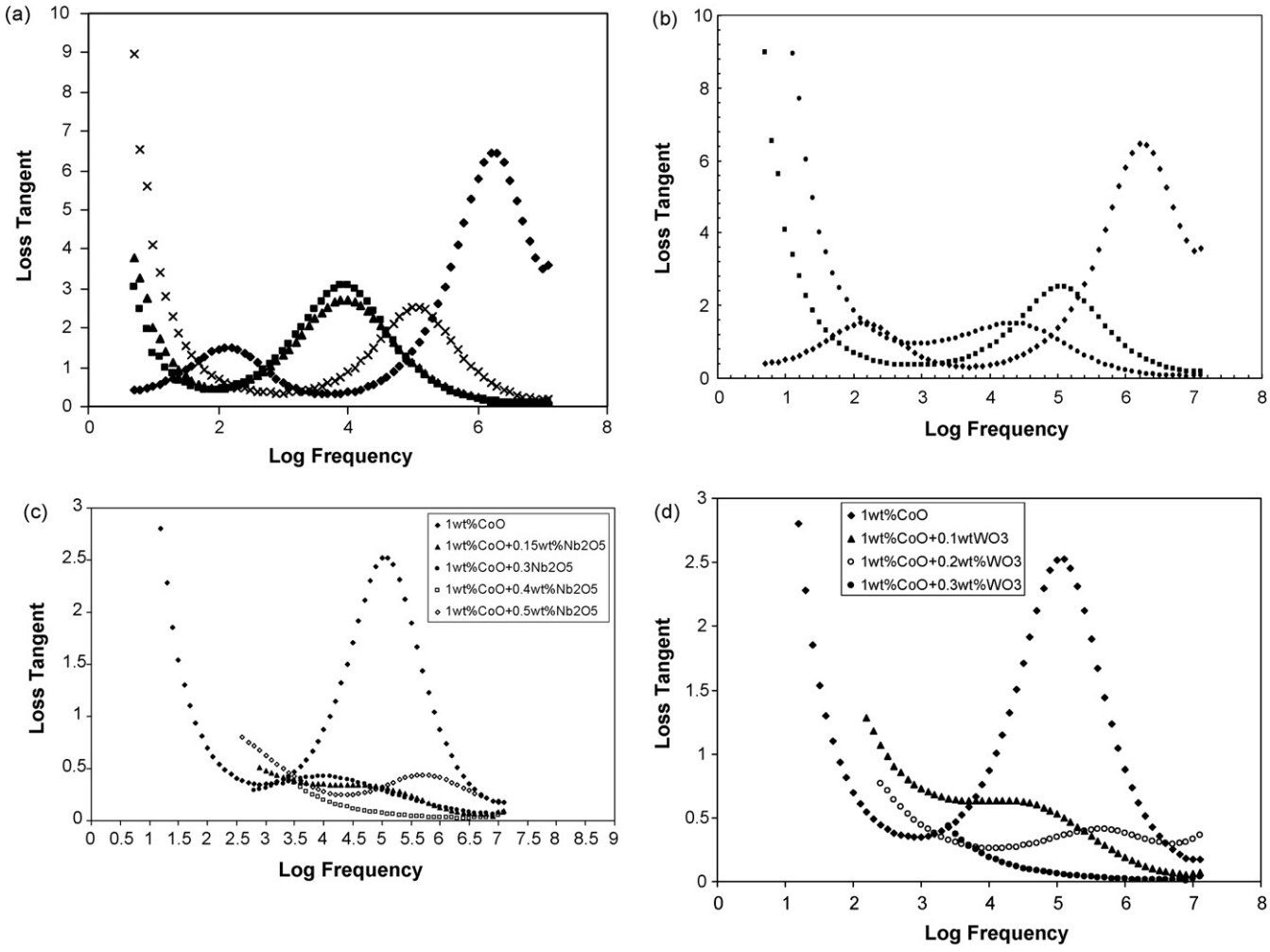

Fig. 10. (a) Dielectric loss tangent for undoped $BiFeO_3$ (♦) and samples prepared with 1% CoO (×), 1% ZnO (▲) or 1% NiO (■) as a function of frequency at room temperature, (b) dielectric loss tangent for undoped $BiFeO_3$ (♦) and samples prepared with 1% CoO via mixed oxide route (■) or chemical route (●) function of frequency at room temperature, (c) dielectric loss tangent data for $BiFeO_3$ samples prepared with $1\%CoO + xNb_2O_5$ as a function of frequency, where $x = 0$ (♦), 0.15 (□), 0.3 (●), 0.5 (◊). (d) Dielectric loss tangent for $BiFeO_3$ prepared with $1\%CoO + x\%WO_3$ samples as a function of frequency where $x = 0$ (♦), 0.1 (□), 0.2 (◯), 0.3 (●).

states of the Fe ion ($Fe^{3+}$and Fe^{2+}), as confirmed by X-ray photoelectron spectroscopy.[5] Buscaglia et al.[12] suggested that the multiple valences lead to the generation of oxygen vacancies to preserve local electrical neutrality and there can be thermally activated hoping from the generated oxygen vacancies.

Losses associated with the space charge relaxation mechanism (<100 Hz) increased with increasing levels of cobalt oxide. In part this is related to the reduction in grain size and the associated increase in the volume of grain boundaries. In a study of grain size effects in $LaAsO_4$, Pradhan and Choudhary[27] demonstrated that increased levels of loss at low frequencies corresponded to space charge polarization from an increasing number of grain boundaries.

Adding cobalt at increasing levels caused a small reduction in the ionic relaxation peak and a displacement of the peak towards lower frequencies (Fig. 10b). This was enhanced for chemically prepared samples. The changes could indicate a reduction in the number of oxygen vacancies upon substitution of Co^{3+} for Fe^{2+}, which is consistent with the structural changes noted earlier. Similarly, ZnO and NiO additions gave rise to a reduction and displacement of the ionic relaxation peak towards lower frequencies, but the changes were much greater than for CoO additions. This may be a consequence of the lattice distortions (as Ni for example is substituted for Fe) modifying the distance between neighbouring oxygen sites. Any change in interatomic distance may alter the resonance frequency for the relaxation mechanism. Liu et al.[28] proposed such a mechanism to explain the displacement in the dielectric loss peak for thin film $BiFeO_3$ samples when subjected to differing annealing temperatures.

In the case of double additions, it is inferred from cell parameter changes that small amounts of Nb^{5+} and W^{6+} ions (ionic radii 64 and 60 pm, respectively) replace the predominant Fe^{3+} on octahedral sites. Dielectric loss data for $BiFeO_3 + 1\%CoO$ samples prepared with different levels of Nb_2O_5 and WO_3 additions are presented in Fig. 10c and d, respectively. Both higher valency additions reduced the high frequency (ionic) relaxation peak significantly. It is noted that the optimum reduction for both Nb^{5+} and W^{6+} additions was achieved at 0.3 wt%, and indeed

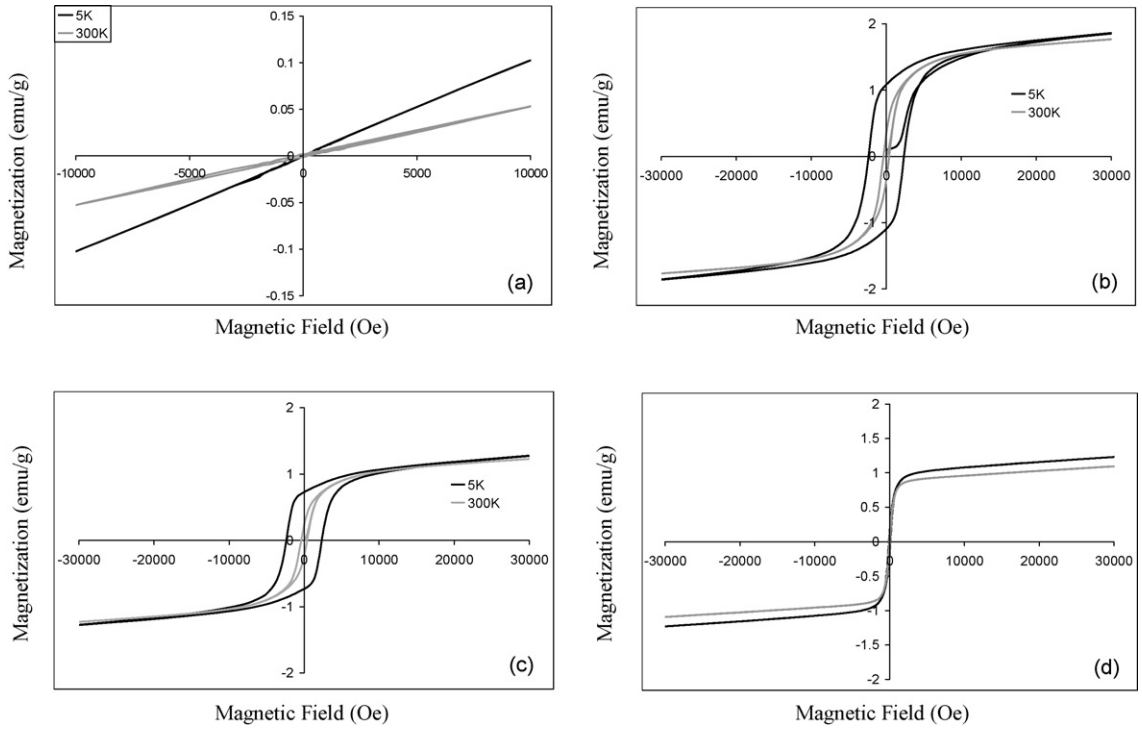

Fig. 11. Magnetization-magnetic field hysteresis data at 5 and 300 K for: (a) undoped $BiFeO_3$, (b) $BiFeO_3$ prepared with 1% CoO addition, (c) $BiFeO_3$ prepared with 0.8% CoO addition and (d) $BiFeO_3$ prepared with 1% NiO addition.

higher levels caused an increase in tan δ (for example Fig. 10c) and the level of internal porosity. It is believed that the primary reason for the reduction in the dielectric loss is a reduction in oxygen vacancy concentration as Nb^{5+} and W^{6+} ions replace Fe^{3+}. Chung et al.[29] and Yu et al.[30] examined current density data for $BiFeO_3$ samples doped with Nb^{5+} and V^{5+}. From the reduction in leakage current they concluded the oxygen vacancy concentration must be reduced by the pentavalent doping. Proposed defect equations for the substitution of Fe^{3+} by Nb^{5+} and W^{6+} additions are presented in Eqs. (1) and (2):

$$Bi_2O_3 + Nb_2O_5 + 2V_O^{\bullet\bullet} \rightarrow 2Bi_{Bi}^{x} + 2Nb_{Fe}^{\bullet\bullet} + 6O_O^{x} + 2O_O^{x} \quad (1)$$

$$Bi_2O_3 + 2WO_3 + 3V_O^{\bullet\bullet} \rightarrow 2Bi_{Bi}^{x} + 2W_{Fe}^{\bullet\bullet\bullet} + 6O_O^{x} + 3O_O^{x} \quad (2)$$

3.7. Magnetic properties

Fig. 11 shows magnetization data collected at 5 and 300 K for undoped $BiFeO_3$ and CoO/NiO-added samples. The simple linear relationships in Fig. 11a confirm that the undoped sample is antiferromagnetic, whilst the hysteresis loops in Fig. 11b–d demonstrates that the CoO- and NiO-added samples are ferromagnetic. In all the ferromagnetic samples, saturation has been achieved by 30 kOe, with values in the range 1.1–1.8 emu/g. Values of the remanent magnetization (M_R) for $BiFeO_3$ samples with 1% CoO additions were 1.08 and 0.35 emu/g at temperatures of 5 and 300 K, respectively. Samples prepared with lower levels of Co additions (0.8%CoO) showed corresponding lower levels of M_R with values of 0.73 and 0.23 emu/g. The NiO-added samples exhibited very narrow ferromagnetic hysteresis loops (Fig. 11d), and the remanent magnetization was significantly reduced (compared to the CoO added samples) to 0.15 and 0.08 emu/g at 5 and 300 K, respectively.

The ferromagnetic data for CoO- and NiO-added samples (Fig. 11) are similar to the results presented by Lópeza et al.,[31] Liu et al.[32] and Duque et al.[33] for the magnetic properties of $CoFe_2O_4$ and $NiFe_2O_4$ nanoparticles. In view of the presence of cobalt and nickel spinel particles, of dimensions up to 10 μm, in the present samples it is concluded that the ferromagnetic behaviour is dominated by the spinel phase rather than the $BiFeO_3$ matrix phase.

The use of a double addition, combining Co and Nb did not have any significant effect on the magnetic properties; the hysteresis data for $BiFeO_3 + 1.0\%CoO + 0.3\%Nb_2O_5$ (Fig. 12) is very similar to that obtained for $BiFeO_3 + 1.0\%CoO$ (Fig. 11b). As an alternative to CoO or NiO, the use of ZnO additions was

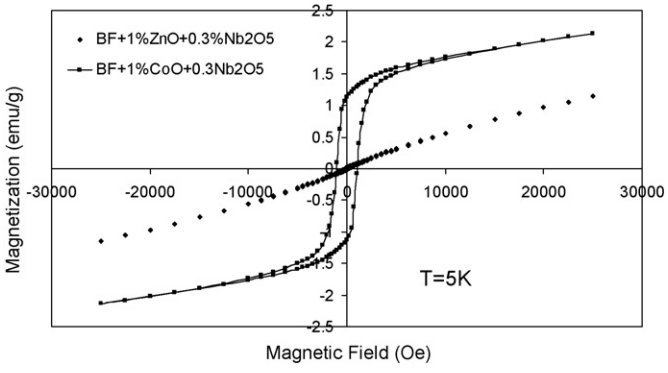

Fig. 12. Magnetization-magnetic field hysteresis data at 5 K for $BiFeO_3 + 1.0\%CoO + 0.3\%Nb_2O_5$ and $BiFeO_3 + 1.0\%ZnO + 0.3\%Nb_2O_5$.

explored. Zinc oxide in the presence of Fe_2O_3 forms a spinel phase which is isostructural with $CoFe_2O_4$ and $NiFe_2O_4$.[34] It was therefore expected that ZnO additions would perform a similar role to that of CoO and NiO additions whereby excess iron would be trapped within the spinel $ZnFe_2O_4$ secondary phase, preventing the formation of $Bi_2Fe_4O_9$. However, as Zn is non-magnetic, there should be little influence on the overall magnetic properties of the sintered sample. This was found to be true; with the magnetic properties of $BiFeO_3 + 1.0\%ZnO + 0.3\%Nb_2O_5$ samples exhibiting antiferromagnetic behaviour (Fig. 12) in a similar manner to the undoped specimens. This confirms that ZnO additions can help prevent formation of the $Bi_2Fe_4O_9$ secondary phase and the spinel second phase does not mask the magnetic properties of the host $BiFeO_3$.

There remains the paradox that it is difficult to sinter bulk $BiFeO_3$ ceramics to high density without the aid of additives such as Co or Ni. Small additions of cobalt oxide in the presence of iron oxide are likely to form the spinel phase $CoFe_2O_4$ which even at nanoparticles size can exhibit ferromagnetic behaviour. Identifying the magnetic characteristics of the primary matrix phase can therefore be difficult. Sintering and densification is not a problem in the case of thin film $BiFeO_3$[35] but much fundamental understanding can gain from the bulk ceramic material provided that the roles of the component phases can be isolated.

4. Conclusions

High density $BiFeO_3$ ceramics (up to 95% theoretical) were prepared with the aid of additions of CoO, ZnO or NiO (up to 1.0%). Such additions led to the formation of the secondary phases ($CoFe_2O_4$, $NiFe_2O_4$ and $ZnFe_2O_4$, respectively); $Bi_{25}FeO_{39}$ was also present in all doped samples. The development of the spinel phase helped to trap excess iron, preventing formation of the $Bi_2Fe_4O_9$ phase. HRTEM revealed the presence of domain structures with stripe configurations in $BiFeO_3$. The domain width is typically 200 nm and $\{1\,1\,0\}$ boundaries are predominant.

Electrical conductivity data for the samples exhibited a clear trend of increasing resistance and increasing activation energy in moving from undoped $BiFeO_3$, to a single additive (Co, or Ni or Zn), to double additives (Co plus Nb or W). The additives provide a means of increasing the resistance by several orders of magnitude.

Small amounts of Co and Ni were accommodated in the matrix phase causing a reduction in the rhombohedral cell parameter. The substitutions also caused a slight reduction in the dielectric loss peaks associated with ionic relaxation. A plausible mechanism is that trivalent Co and Ni ions replace Fe^{2+} ions, with a reduction in the population of oxygen vacancies to maintain charge neutrality. Additions of higher valance species (Nb^{5+} and W^{6+}) along with Co or Ni led to a complete removal of the dielectric loss peak associated with ionic relaxation.

The undoped $BiFeO_3$ was antiferromagnetic, but all samples prepared with Co/Ni additions were ferromagnetic, reflecting the presence of $CoFe_2O_4$ and $NiFe_2O_4$ grains or indeed nanoparticles within the microstructure. Only when samples were prepared with ZnO additions was antiferromagnetic behaviour observed again. The non-magnetic spinel $ZnFe_2O_4$ developed in the samples by trapping excess iron and preventing the formation of $Bi_2Fe_4O_9$.

Acknowledgements

The financial support of EPSRC through GR/T19148, the provision of an EPSRC Doctoral Training Award to Michael Thrall, and the assistance of Daresbury Laboratory staff with synchrotron radiation X-ray diffraction studies are gratefully acknowledged. Dr David Hall is thanked for helpful discussions on the defect equations.

References

1. Kimura, T., Kawamoto, S., Yamada, I., Takano, M. and Tokura, Y., Magnetocapacitance in multiferroic $BiMnO_3$. *Phys. Rev. B*, 2003, **67**, 180401.
2. Eerenstein, W., Mather, N. D. and Scott, J. F., Multiferroic and magnetoelectric materials. *Nature*, 2006, **442**, 759–765.
3. Pradhan, A. K., Zhang, K., Hunter, D., Dadson, J. B., Loiutts, G. B., Bhattacharya, P. *et al.*, Magnetic and electrical properties of single-phase multiferroic $BiFeO_3$. *J. Appl. Phys.*, 2005, **97**, article 093903.
4. Kadomtseva, A., Zvezdin, A. K., Popov, Y. F., Pyatakov, A. P. and Vorob'ev, G. P., Space-time parity violation and magnetoelectric interactions in antiferromagnets. *JETP Lett.*, 2004, **79**, 571–581.
5. Wang, Y. P., Zhou, L., Zhang, M. F., Chen, X. Y., Liu, J. M. and Liu, Z. G., Room temperature saturated ferroelectric polarization in $BiFeO_3$ ceramics synthesized by rapid liquid phase sintering. *Appl. Phys. Lett.*, 2004, **84**, 1731–1733.
6. Thrall, M., The magnetic, electric and structural properties of multiferroic $BiFeO_3$ and $BiMnO_3$. *PhD thesis*, The University of Manchester, 2008.
7. Achenbach, G. D., James, W. J. and Gerson, R., Preparation of single-phase polycrystalline $BiFeO_3$. *J. Am. Ceram. Soc.*, 1967, **50**, 437.
8. Seblach, S. M., Einarsrud, M.-A. and Grande, T., On the thermodynamic stability of $BiFeO_3$. *Chem. Mater.*, 2009, **21**, 169–173.
9. Zhang, S. T., Lu, M. H., Wu, D., Chen, F. and Ming, N. B., Larger polarization and weak ferromagnetism in quenched $BiFeO_3$ ceramics with a distorted rhomohedral crystal structure. *Appl. Phys. Lett.*, 2005, **87**, article 262907.
10. Kumar, M. M., Palker, V. R., Srinivas, K. and Suryanarayana, S. V., Ferroelectricity in a pure $BiFeO_3$ ceramics. *Appl. Phys. Lett.*, 2000, **76**, 2764–2766.
11. Nalwa, K. S., Grag, A. and Upadhyaya, A., effect of samarium doping on the properties of solid state synthesized multiferroic bismuth ferrite. *Mater. Lett.*, 2008, **62**, 878–881.
12. Buscaglia, M. T., Mitoseriu, L., Pellechi, L., Buscaglia, V., Viviani, M. and Siri, A. S., Preparation and characterisation of the magnetoelectric $x BiFeO_3$–$(1-x)BaTiO_3$ ceramics. *J. Eur. Ceram. Soc.*, 2006, **26**, 3027–3030.
13. Singh, K., Negri, N. S., Kotnala, R. K. and Singh, M., Dielectric and magnetic properties of $(BiFeO_3)_{1-x}(PbTiO_3)_x$ ferromagnetoelectric system. *Solid State Commun.*, 2008, **148**, 18–21.
14. Kumar, M. M., Srinivas, A. and Suryanarayana, S. V., Structure property relations in $BiFeO_3/BaTiO_3$ solid solutions. *J. Appl. Phys.*, 2000, **87**, 855–862.
15. Jun, Y. K., Moon, W. T., Chang, C. M., Kim, H. S., Ryu, H. S., Kim, J. W. *et al.*, Effects of Nb-doping on electric and magnetic properties in muti-ferroic $BiFeO_3$ ceramics. *Solid State Commun.*, 2005, **135**, 133–137.
16. Jun, Y. K. and Hong, S.-H., Dielectric and magnetic properties in Co- and Nb-substituted $BiFeO_3$ ceramics. *Solid State Commun.*, 2007, **144**, 329–333.
17. Ricote, J., Whatmore, R. W. and Barber, D. J., Studies of the ferroelectric domains configuration and polarization of rhombohedral PZT ceramics. *J. Phys. Condens. Matter*, 2000, **12**, 323–337.
18. Pechini, M. P., *US Patent. 3330697*, 1967.
19. *TOPAS software (Ver. 2.1)*. Bruker AXS Ltd., Coventry, UK, 2003.

20. Carvalo, T. T. and Tavares, P. B., Synthesis and thermodynamic stability of multiferroic $BiFeO_3$. *Mater. Lett.*, 2008, **62**, 3984–3986.
21. Valant, M., Axelsson, A.-K. and Alford, N., Peculiarities of a solid-state synthesis of multiferroic polycrystalline $BiFeO_3$. *Chem. Mater.*, 2007, **19**, 5431–5436.
22. Shannon, R. D., Revised effective ionic radii and systematic studies of interatomic distances in halides and chalcogenides. *Acta Cryst.*, 1976, **A32**, 751–767.
23. Fousek, J. and Janovec, V., The orientation of domain walls in twinned ferroelectric crystals. *J. Appl. Phys.*, 1969, **40**, 135–142.
24. Woodward, D. I., Reaney, I. M., Eitel, R. E. and Randall, C. A., Crystal and domain structure of the $BiFeO_3$–$PbTiO_3$ solid solution. *J. Appl. Phys.*, 2003, **94**, 3313–3318.
25. Chen, Y. B., Katz, M. B., Pan, Q. X., Das, R. R., Kim, D. M., Baek, S. H. *et al.*, Ferroelectric domain structures of epitaxial (0 0 1) $BiFeO_3$ thin films. *Appl. Phys. Lett.*, 2007, **90**, article 072907.
26. Randall, C. A. and Barber, D. J., What more, ferroelectric domain configuration in a modified PZT ceramic. *J. Mater. Sci.*, 1987, **22**, 925–931.
27. Pradhan, A. K. and Choudhary, R. N. P., Dielectric and thermal properties of $LaAsO_4$. *J. Mater. Sci.*, 1987, **22**, 2955–2958.
28. Liu, H., Liu, Z., Liu, Q. and Yao, K., Ferroelectric properties of $BiFeO_3$ films grown by sol–gel process. *Thin Solid Films*, 2006, **500**(1–2), 105–109.
29. Chung, C. F., Lin, J. P. and Wu, J. M., Influence of Mn and Nb dopants on electric properties of chemical-solution-deposited $BiFeO_3$ films. *Appl. Phys. Lett.*, 2006, **88**, article 242909.
30. Yu, B. F., Li, M. Y., Liu, J., Guo, D. Y., Pei, L. and Zhao, X. Z., Effects of ion doping at different sites on electrical properties of multiferroic $BiFeO_3$ ceramics. *J. Phys. D Appl. Phys.*, 2008, **41**, article 065003.
31. Lópeza, J. L., Pfannes, H. D., Paniago, R., Sinnecker, J. P. and Novak, M. A., Investigation of the static and dynamic magnetic properties of $CoFe_2O_4$ nanoparticles. *J. Magnet. Magnet. Mater.*, 2008, **320**, E327–E330.
32. Liu, X. N., Fu, S. X. and Huang, C. S., Synthesis and magnetic characterization of novel $CoFe_2O_4$–$BiFeO_3$ nanocomposites. *Mater. Sci. Eng. B*, 2005, **121**, 255–260.
33. Duque, J. G. S., Souza, E. A., Meneses, C. T. and Kubota, L., Magnetic properties of $NiFe_2O_4$ nanoparticles produced by a new chemical method. *Phys B*, 2007, **398**, 287–290.
34. Schaefer, W., Kockelmann, W., Kirfel, A., Potzel, W., Burghart, F. J., Kalvius, G. M. *et al.*, Structural and magnetic variations of $ZnFe_2O_4$ spinels neutron powder diffraction studies, European Powder Diffraction, Parts 1 and 2. *Mater. Sci. Forum*, 2000, **321–3**, 802–807.
35. Srivastava, A., Grag, A. and Morrison, F. D., Impedance spectroscopy studies on polycrystalline $BiFeO_3$ thin films on Pt/Si substrates. *J. Appl. Phys.*, 2009, **105**, article 054103.